Applied Physics Letters

Anisotropy-induced spin disorder in intergrown, ferrimagnetic Fe_7S_8 polytypes

Cite as: Appl. Phys. Lett. **121**, 154103 (2022); https://doi.org/10.1063/5.0111498
Submitted: 19 July 2022 • Accepted: 21 September 2022 • Published Online: 11 October 2022

Alexander Firlus, Jürgen E. K. Schawe, Peter G. Weidler, et al.

Applied Physics Letters ARTICLE scitation.org/journal/apl

Anisotropy-induced spin disorder in intergrown, ferrimagnetic Fe_7S_8 polytypes

Cite as: Appl. Phys. Lett. **121**, 154103 (2022); doi: 10.1063/5.0111498
Submitted: 19 July 2022 · Accepted: 21 September 2022 ·
Published Online: 11 October 2022 · Publisher error corrected: 11 October 2022

Alexander Firlus,[1,a] Jürgen E. K. Schawe,[1,2] Peter G. Weidler,[3] Michalis Charilaou,[4] Jörg F. Löffler,[1] and Andreas U. Gehring[1,a]

AFFILIATIONS

[1]Laboratory of Metal Physics and Technology, Department of Materials, ETH Zurich, 8093 Zurich, Switzerland
[2]Mettler-Toledo GmbH, Analytical, 8606 Nänikon, Switzerland
[3]Institute of Functional Interfaces, Karlsruhe Institute of Technology, 76344 Eggenstein-Leopoldshafen, Germany
[4]Department of Physics, University of Louisiana at Lafayette, Lafayette, Louisiana 70504, USA

[a]Authors to whom correspondence should be addressed: alexander.firlus@mat.ethz.ch and agehring@ethz.ch

ABSTRACT

The monosulfides of the pyrrhotite omission series ($Fe_{1-x}S$, $0 < x \leq 0.125$) are important remanence carriers for paleomagnetic reconstruction of the Earth's crust and extraterrestrial materials. The ferrimagnetic Fe_7S_8 polytypes are the endmembers, and their stacking modulations of full and vacant layers generate different magnetic anisotropy properties due to the cation-vacancy configurations. In this study, intergrown long-range ordered polytypes with four- and threefold modulation, i.e., 4C and 3C pyrrhotite, were prepared in a diffusion-driven process by quenching of a natural pyrrhotite crystal with randomized vacancies. In addition, a third constituent with coherence lengths of a few nanometers, denoted 3C*, was found that exhibits spin-glass behavior at about 10 K due to local magnetic anisotropies arising from vacancy-density variations. The concomitant occurrence of this nano-scale constituent with spin disorder and the long-range ordered polytypes indicate competitive diffusion-driven processes during Fe_7S_8 formation. Such information provides insight into the provenance and genesis of ferrimagnetic pyrrhotite in Earth and extraterrestrial systems and in a broader sense into vacancy-induced materials.

The interplay between structure and magnetic properties in solids is of special importance for the identification, comprehension, and development of possible functionality of materials for scientific and technological applications. In this context, effects emerging due to vacancies that cause changes in crystallographic symmetry and/or magnetic order are of fundamental interest.[1–3] Earth-abundant iron monosulfides of the pyrrhotite group ($Fe_{1-x}S$, $0 < x \leq 0.125$) are an ideal crystallographic testing ground to explore vacancy-induced magnetism, because vacancies can be arranged in different configurations that generate commensurate and incommensurate phases with variable physical and chemical properties.[4] The iron-deficient Fe_7S_8 endmember occurs in two ferrimagnetic polytypes with threefold and fourfold stacking modulation of full and vacancy layers that stem from the distribution of vacant octahedral sites in a hexagonally closed packing of sulfur and are denoted 3C and 4C pyrrhotite, respectively.[5,6] The mineralogical and physical properties of the latter have been extensively studied because it is a key magnetic remanence carrier in the Earth's crust and extraterrestrial materials for paleomagnetic reconstructions.[7–10] In contrast, 3C pyrrhotite has rarely been reported and it is mainly known from recent gas-hydrate bearing sedimentary deposits.[11] Both polytypes have also been synthesized.[6,12–14] In recent years, Fe_7S_8 syntheses for technical applications gained increasing interest and it has been shown that the magnetic properties are sensitive to crystallite size and vacancy order.[12,15–18] Furthermore, superstructure changes within the pyrrhotite group are controlled by vacancy diffusion.[12,19,20] Both polytypes transform into a paramagnetic 1C phase with randomly distributed vacancies at a temperature of approximately 600 K.[4,13] The 1C to 4C transition is reversible, but the relaxation kinetics to reach perfect vacancy ordering occurs over geological time frames.[21] Moreover, the absence of the natural 3C pyrrhotite in the pre-Holocene (>11 700 years) is probably due to its metastability with respect to 4C pyrrhotite.

The two Fe_7S_8 polytypes derive from a hexagonal NiAs-type substructure and their vacancy order generates two different superstructures (Fig. 1). In the higher-ordered 4C polytype with monoclinic unit cell (space group $C2/c$), the 32 cations occupy the two sites Fe1 and

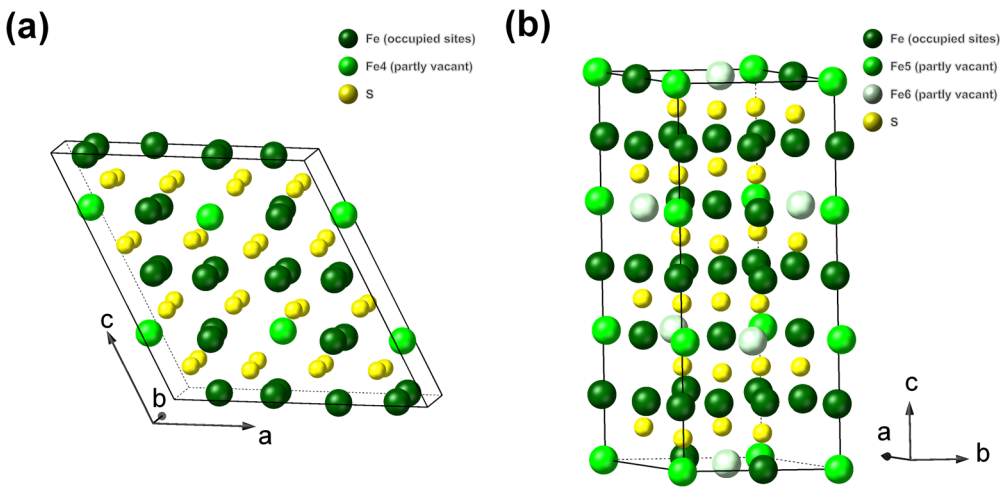

FIG. 1. Unit cells of 4C and 3C pyrrhotite. (a) 4C pyrrhotite consisting of fully occupied sites of Fe (dark green) and half-filled Fe4 vacancy sites (light green). (b) 3C pyrrhotite with fully occupied sites of Fe (dark green) and stochastically occupied sites of Fe5 (light green) and Fe6 (gray-green).

Fe3 in the full layers and Fe2 and Fe4 in the vacancy layers, where only half of the Fe4 sites is filled.[5,22–24] Doubling the unit cell along the *c*-axis generates a centrosymmetric superstructure with a fourfold modulated stacking sequence. In contrast, the distorted trigonal 3C polytype (space group $P3_121$) is non-centrosymmetric with the three sites Fe1, Fe2, and Fe3 in the full layers and Fe4, Fe5, and Fe6 in the vacancy layers [Fig. 1(b)]. The latter two sites are vacant with a statistical probability inferred at about 15% for Fe5 and 85% for Fe6,[14] i.e., two vacancy sites can be next neighbors with a probability of about 12% [Fig. 1(b)].

In the 3C and 4C polytypes, the ferrimagnetism stems from uncompensated sublattices within the stacking sequence, where intralayer spins are ferromagnetically (FM) and adjacent inter-layer spins are antiferromagnetically (AFM) coupled.[4,25,26] For the 4C pyrrhotite, a theoretical value for the saturation magnetization of $M_s \approx 21\ \mathrm{A\,m^2\,kg^{-1}}$ was predicted.[25] Moreover, this polytype has a characteristic anisotropy with an easy *c*-plane and a hard *c*-axis.[27] Based on theoretical considerations of the NiAs-type structure by Goodenough,[28] the spin–orbit coupling (SOC) due to covalency of Fe–Fe bonds of less than 3 Å can explain the peculiar anisotropy traits. All interlayer Fe–Fe bonds are below this critical value and a magnetic anisotropy energy of $E_{MA} = 5.49$ meV per unit cell has been reported.[22,29] This results in a spin rotation out of the easy plane and in an intrinsic magnetic anomaly at about 32 K, known as Besnus transition.[23,30–32] The spin rotation is incoherent and it can be linked to vacancy order, which generates two anisotropy systems offset by 30°.[33–35] Koulialias *et al.*[34] demonstrated that the coupling between the two systems marks the Besnus transition. Moreover, Haines *et al.*[26] predicted a spin-flop transition for the lesser-ordered 3C polymorph.

In this study, we generate a structure of intergrown 4C and 3C polytypes by thermal treatment of a natural pyrrhotite and the link between structural and magnetic traits is used to provide insights into the vacancy ordering of a defect-supported magnetic material.

The initial material is a well-described natural pyrrhotite crystal from Auerbach (Germany) that consists of 4C and 5C* pyrrhotite phases with a chemical bulk composition of $Fe_{6.6}S_8$.[36,37] The thermal conversion was conducted in a Mettler Toledo DSC 1 by heating crystal flakes of 17–19 mg to 650 K at 10 K/min followed by cooling to room temperature at the same rate. Powder x-ray diffraction (XRD) with CuK_α radiation was performed at room temperature to identify the phases in the sample before and after the thermal treatment. The TOPAS software was used for the Rietveld refinement of the XRD data.[38,39] Detailed analysis and visualization of the structural data were made with the Crystal Maker software. The behavior of the magnetization in a 3 T field (M_{3T}) of both samples between 300 and 5 K was investigated with a Quantum Design Magnetic Property Measurement System (MPMS3). The samples were oriented along the easy *c*-plane of the 4C pyrrhotite. The complex susceptibility $\chi^*(\omega) = \chi'(\omega) - i\chi''(\omega)$ was measured in AC fields with 800 A/m superimposed by a 0.1 T DC bias field at frequencies f between 5 and 200 Hz.

Atomic-scale characterization of the starting, intergrown 4C and 5C* superstructures,[36,37] revealed an incommensurate 4.91C pyrrhotite, which cannot be chemically differentiated from the intergrown 4C pyrrhotite.[37] Rietveld refinement of the 4C phase using the structural model of Powell *et al.*[13] yields for the untreated sample the unit-cell parameters $a = 11.9134 \pm 0.0003$ Å, $b = 6.8701 \pm 0.0002$ Å, $c = 12.9074 \pm 0.0004$ Å, and $\beta = 118.047 \pm 0.001°$ with a Bragg factor of $R_{Bragg} = 5.5$. Using the model of Elliot,[40] the refined monoclinic 5C* phase ($P21/c$) has a unit cell with $a = 6.8910 \pm 0.0004$ Å, $b = 28.649 \pm 0.0009$ Å, $c = 6.8852 \pm 0.0003$ Å, and $\beta = 119.9309° \pm 0.004°$ with $R_{Bragg} = 5.6$. The Rietveld refinement of the diffractogram has a goodness of fit (GOF) of 3.41.

After heating the sample to 650 K, the XRD pattern at room temperature exhibits no 5C* peaks (Fig. 2). This accords with thermomagnetic data by Koulialias[41] that reveal at $T \approx 495$ K an irreversible 5C* phase transition into a ferrimagnetic phase. In the thermally treated sample, the Bragg peaks and the relatively pronounced background at $2\theta < 60°$ can be attributed to 4C and newly formed 3C pyrrhotite (Fig. 2). The 4C unit-cell parameters using the same structural model as above are $a = 11.9118 \pm 0.0004$ Å, $b = 6.8723 \pm 0.0002$ Å, $c = 12.9080 \pm 0.0003$ Å, and $\beta = 117.983 \pm 0.002°$ with $R_{Bragg} = 2.2$. These parameters exhibit no significant changes compared to the initial

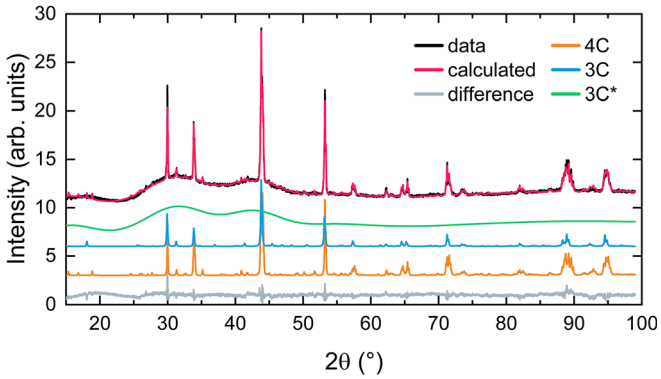

FIG. 2. XRD diffractogram for the thermally treated sample. The measured and calculated patterns and their difference curve are shown. The diffractogram arises from superimposed Bragg peaks of 4C and 3C pyrrhotite and broad features assigned to a disordered, small-sized 3C* constituent.

sample. The newly formed 3C pyrrhotite was refined with the model by Keller-Besrest *et al.*[14] in the space group $P3_121$ and yielded unit-cell parameters of $a = 6.8848 \pm 0.0003$ Å and $c = 17.1472 \pm 0.0011$ Å with $R_{Bragg} = 2.1$. The background modulations with broad peaks generally stem from poorly ordered crystallites that are small in size and/or reveal a lattice distortion. Taking the structural parameters for 3C pyrrhotite into account when performing the Rietveld refinement, the modulation can be well described by the Keller-Besrest model.[14] However, a better agreement between the measured and refined background, as indicated by the decrease in the GOF from 6.2 to 2.3, is obtained by the model of Nakano *et al.*,[6] which rests upon the same space group but describes a slightly different vacancy distribution in the 3C pyrrhotite (Fig. 2). The refinement reveals a 3C polytype with a coherence length of a few nanometers, i.e., of one to three unit cells. To distinguish this perturbed, small-sized phase from the long-range ordered 3C pyrrhotite, it is denoted 3C* in analogy to the identification of the incommensurate 5C* pyrrhotite.[36,37] The GOF of 2.3 obtained from the refinement of the XRD pattern shows that the thermally treated sample is well described as an intergrowth of 4C, 3C, and 3C* polytypes. The concomitant occurrence of the three polytypes indicates the formation of cation vacancy configurations that locally minimize the free energy in the quenched material. In such a process, areas with minimized free energy are separated by boundaries with higher free energy and the small-sized, disordered 3C* constituent appears to be a likely candidate to form this kind of boundary.

At 300 K, the initial sample has a magnetization in a 3 T field of $M_{3T} = 16.8\ \mathrm{A\,m^2\,kg^{-1}}$ [Fig. 3(a)]. Neglecting the magnetic contribution of the antiferromagnetic 5C* phase and considering the theoretical value of $M_s \approx 21\ \mathrm{A\,m^2\,kg^{-1}}$ for 4C pyrrhotite,[25] the latter is the dominant phase with about 75%. After thermal treatment, the new composition with 4C, 3C, and 3C* pyrrhotite increased M_{3T} to $18.4\ \mathrm{A\,m^2\,kg^{-1}}$. The 4C and 3C pyrrhotite are both ferrimagnetic, whereas in the 3C* constituent with an average coherence length of a few nanometers, the ferrimagnetic order is perturbed due to structural disorder. Given this, M_{3T} stems mainly from 4C and 3C pyrrhotite.

For the initial sample, the temperature dependence of M_{3T} between 300 and 50 K can be described by a second-order polynomial with a maximum at about 165 K [Fig. 3(a)]. At lower temperature, the local maximum at $T \approx 25$ K is attributed to the Besnus transition.[36] This intrinsic low-temperature behavior was explained by the interplay of the Zeeman energy E_Z and the magnetocrystalline anisotropy energy E_{MA}.[34] The maximum in M_{3T} marks the beginning of a pronounced out-of-plane spin rotation where the change in the anisotropy energy ΔE_{MA} exceeds E_Z. This coincides with the shortening of intra-layer Fe3–Fe3 bonds below the critical value of 3 Å and a change in sign of the anisotropy constant K_3.[13,30,33,34] The M_{3T} curve for the thermally treated sample can also be described by a second-order polynomial between 300 and 50 K. The quadratic terms of both curves are identical. Thus, a vertical and a horizontal shift by 16.5 K to higher temperature and lowering M_{3T} by $1.98\ \mathrm{A\,m^2\,kg^{-1}}$ makes the polynomial curves congruent. The nearly linear difference of the measured

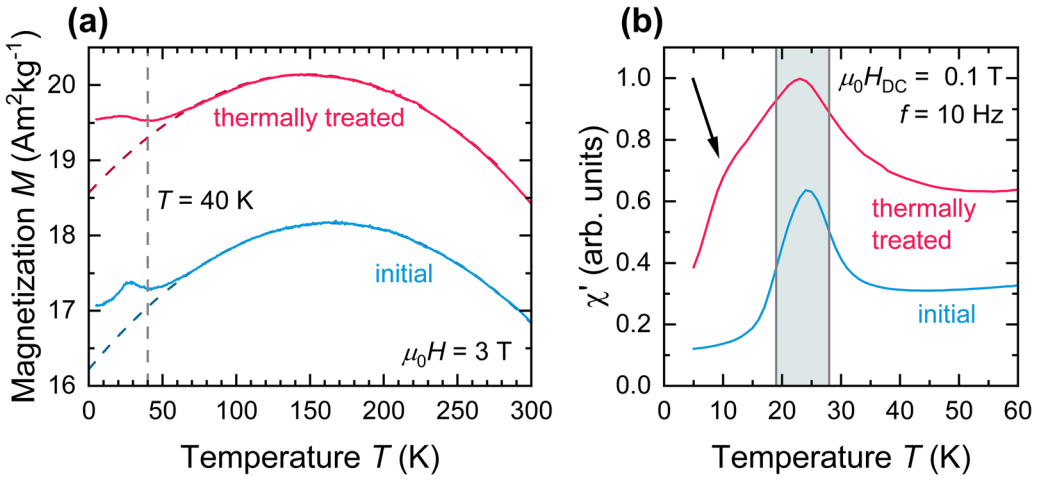

FIG. 3. Magnetization and magnetic susceptibility of the initial and thermally treated samples. (a) Field-cooled magnetization curves and polynomial fits for $T > 50$ K (dashed lines). (b) The magnetic susceptibility around the Besnus transition of the heat-treated sample is double that of the initial sample. At the Besnus transition, the curve can be fitted with a Lorentzian function (marked in gray). The curve for the thermally treated sample has a broad shoulder (arrow).

curves in this temperature range suggests no spin-flop for the 3C phase in a field of 3 T.

As mentioned above, the out-of-plane rotation in 4C pyrrhotite results from the interplay of the covalent Fe–Fe bonds and the ordered vacancy arrangements. The monoclinic superstructure consists of chain elements parallel to the *c*-axis with seven cations that are separated by a vacancy.[23,24] All the Fe–Fe bonds in these chains are covalent and contribute to the SOC. In 3C pyrrhotite, the interlayer Fe–Fe bonds are also covalent but the stochastic occupation of the Fe5 and Fe6 sites fragments the chain segments and generates distortions (Fig. 4). Both effects can influence the Fe–Fe bond lengths. This configuration of the covalent Fe–Fe bonds causes local SOC variations in the lattice, which in turn may explain the absence of long-range, collective out-of-plane spin rotations in 3C pyrrhotite as is characteristic of the 4C polytype.

At $T < 50$ K, the peak in M_{3T} indicates the Besnus transition in 4C pyrrhotite, where the two spin rotation systems start to couple.[34,35] Compared to the initial sample, the thermally treated one reveals a broadening of this peak [Fig. 3(a)]. Susceptibility measurements better resolve this effect [Fig. 3(b)]. In both samples, the peak can be fitted with a Lorentzian between 19 and 28 K. The peak broadening is associated with a slight shift from 24 to 23 K. Considering that such a peak occurs for pure 4C pyrrhotite at $T \approx 32$ K,[23,42] the shift to lower temperature can be explained by a local perturbation in the superstructure due to cation disorder on an atomic level.[37] With this in mind, the nearly identical peak positions of the initial and thermally treated samples indicate that the quenching has no critical effect on the vacancy order of the 4C superstructure.

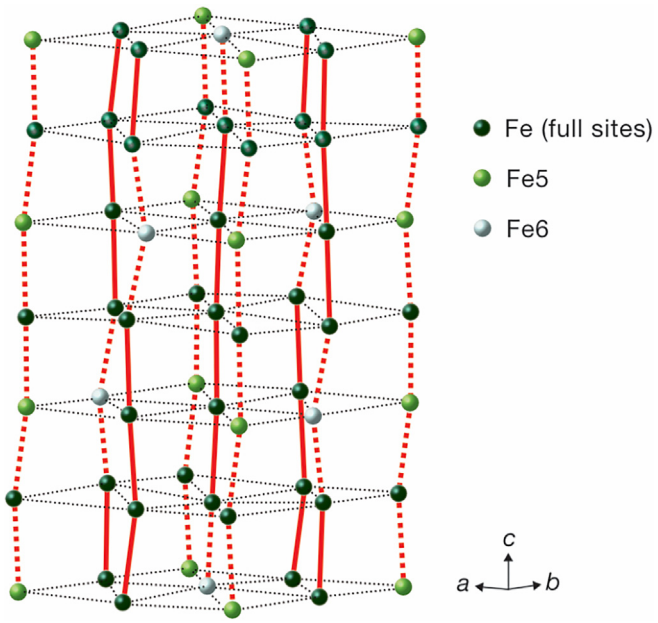

FIG. 4. Framework of Fe sites in a 3C unit cell with fully occupied sites (dark green), vacancies with 15% probability (Fe5, light green) and 85% probability (Fe6, gray-green). Fe–Fe bonds >3 Å (black dotted lines), Fe–Fe bonds <3 Å between full sites (red solid lines), and between full and stochastically occupied sites (red dotted lines) are highlighted.

The magnetic susceptibility of the thermally treated sample is nearly double that of the initial one [Fig. 3(b)]. Because Koulialias[41] showed that the heat treatment only marginally enhances the magnetization in a field of 0.1 T, such a drastic increase cannot be attributed solely to the ferrimagnetic 3C or 4C pyrrhotite in the sample. Therefore, the susceptibility increase mainly stems from 3C* pyrrhotite. In this constituent, the stochastic vacancy distribution and the perturbed stacking modulation make the FM and AFM interactions of the sublattices less constrained with respect to the magnetic orientation of their neighbors and the external field, and this in turn can explain the magnetic relaxation detected in the $\chi^*(T,\omega)$ measurements. The larger values of χ' indicate an increased spin mobility.

The enhanced susceptibility is linked to relaxation, i.e., to a spin–glass transition, at about 10 K [Figs. 5(a) and 5(b)]. The temperature dependence of the effective relaxation time is related to the peak's maximum frequency ω_{max} by $\tau(T) = 1/\omega_{max}$. The relaxation is caused by cooperative spin fluctuations that freeze when the relaxation time exceeds the experimental measurement time at low temperatures. The inflection point of χ' shifts to higher temperatures as the excitation frequency is enhanced and this is well resolved in the χ'' peak. From the measured frequency dependence of the relaxation, an apparent activation energy of $E_a = 23.24 \pm 1.27$ meV (=2.24 kJ/mol) can be determined using the Arrhenius–Néel equation $\tau(T) = \tau_0 \exp(E_a/k_B T)$, where τ is the relaxation time, τ_0 is a pre-exponential factor, E_a is the apparent activation energy, and k_B is the Boltzmann constant [Fig. 5(c)].

An average size of regions with cooperative spin fluctuations is inferred from E_a. Such regions are critically determined by the configuration of covalent Fe–Fe bonds and vacancies that induce localized magnetic anisotropy properties. In 4C and 3C pyrrhotite, these bonds are similar (Fig. 1), and therefore, it is assumed that the SOC and magnetocrystalline anisotropy energy in the two polytypes are of the same magnitude. For 4C pyrrhotite, a magnetocrystalline anisotropy energy of $E_{MA} = 0.2$ meV/Fe atom can be inferred.[29] Given this, $E_a \approx 23$ meV corresponds to cooperative spin fluctuations of about 115 Fe atoms on average, which comprise about three unit cells of the 3C* pyrrhotite (Fig. 4).

From χ'' and the Arrhenius–Néel equation, the relaxation spectrum is determined [Fig. 5(d)], which can be described by the Havriliak–Negami equation,[43,44] $\chi^*(\omega) = \chi_\infty + \frac{\Delta\chi}{(1+(i\omega\tau_{HN})^m)^n}$, where χ_∞ is the limiting susceptibility, $\Delta\chi$ is the intensity of the relaxation transition, τ_{HN} is the Havriliak–Negami relaxation time, and n and m are shape parameters, which correspond to the slopes in Fig. 5(d). The low-frequency slope is m and the high-frequency slope is $-m \times n$.[45] The obtained slopes $m = 0.05$ and $m \times n = 0.12$ are small compared to those of structural glasses,[46] which is indicative of a broad relaxation time distribution. Moreover, cooperative spin rearrangements during the glass transition are characterized by the dynamic fragility[47] $m_d = \frac{1}{T_g}\frac{d\log\tau}{dT^{-1}}\big|_{T_g} = \frac{1}{\ln(10)}\frac{E_a}{T_g k_B}$. Considering the slope of the activation diagram at the glass transition temperature $T_g = 7.1$ K, which is defined as $\tau(T_g) = 100$ s,[48,49] the dynamic fragility is $m_d = 17$. This suggests a strong glass-forming system that can be well described by an Arrhenius–Néel-like activation behavior.[47] The broad shape of the relaxation spectrum and the low dynamic fragility indicate a low cooperativity of the relaxations in the glass-transition region, which is most likely caused by a spatial separation of spin fluctuations. Such regions

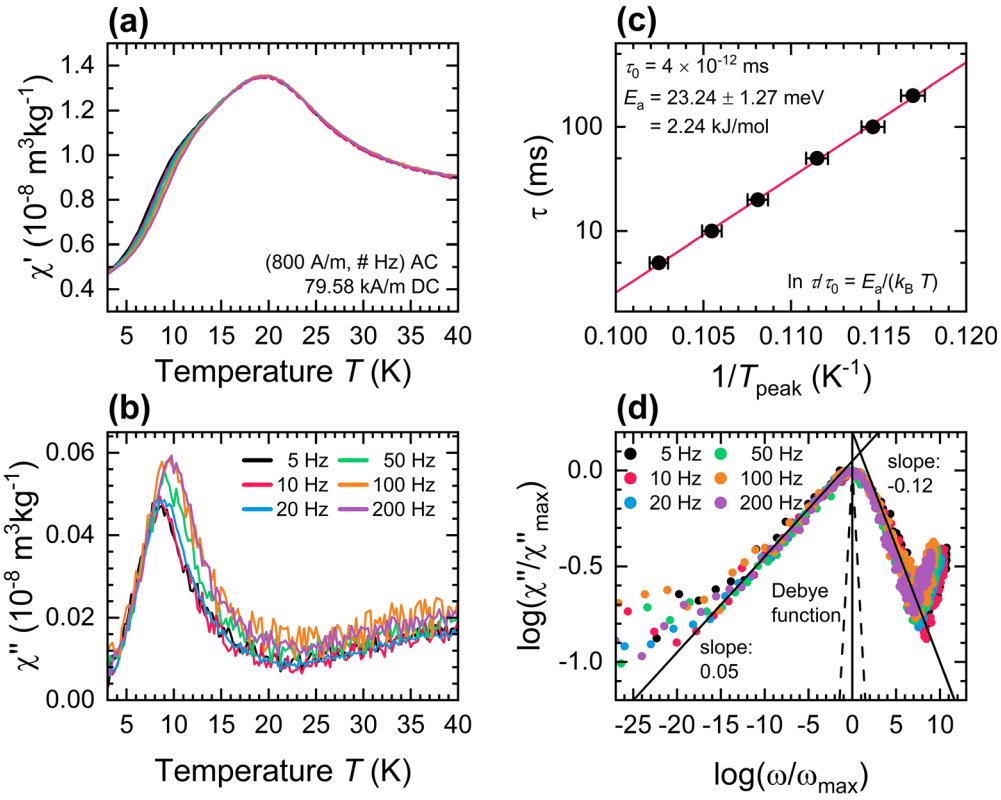

FIG. 5. Magnetic susceptibility of the thermally treated sample. (a) The in-phase component χ' has a slight frequency dependence between 5 and 15 K. (b) The out-of-phase component χ'' has a frequency-dependent peak at $T \approx 10$ K. (c) The peak position of χ'' follows the Arrhenius–Néel law with an activation energy of 2.24 kJ/mol. The error bars correspond to one standard deviation of the fitting process for the peak position in χ''. (d) The broad relaxation spectrum of the spin–glass regions stems from multiple, similar relaxators. A single relaxator case (Debye function) is indicated by dashed lines.

of separated spin fluctuations can be attributed to the disordered 3 C* constituent, randomly distributed in the pyrrhotite crystal.

In summary, thermally induced diffusion-controlled vacancy ordering in natural ferrimagnetic Fe_7S_8 generates 4C and 3C polytypes that are different in the stacking modulation of the cations in the full and vacancy layers. Highly ordered vacancies yield well-defined anisotropy systems in 4C and to a lesser degree in 3C pyrrhotite. The stochastic vacancy order in the 3C polytype can additionally generate small-sized structures, denoted 3C*, which result in disordered, magnetic regions with spin-glass behavior at about 10 K. The 4C, 3C, and 3C* polytypes can be distinguished by dynamic magnetization measurements in concert with structural analysis, which opens a new avenue to characterize vacancy order in Fe_7S_8. This is essential for their use in paleomagnetic reconstructions of Earth and extraterrestrial systems and can provide further insight into vacancy ordering in defect-supported magnetic materials.

This work was supported by an ETH Research Grant (No. ETH-47 17-1).

AUTHOR DECLARATIONS

Conflict of Interest

The authors have no conflicts to disclose.

Author Contributions

Andreas U. Gehring, Jürgen E. K. Schawe, Jörg F. Löffler, and Alexander Firlus designed the study. Alexander Firlus performed the magnetometry experiments. Peter G. Weidler measured and analyzed the x-ray diffraction data. Jürgen E. K. Schawe performed the DSC experiments. Alexander Firlus, Jürgen E. K. Schawe, and Andreas Ulrich Gehring analyzed and correlated the data. All authors discussed and validated the results and wrote the manuscript.

Alexander Firlus: Conceptualization (equal); Formal analysis (equal); Investigation (equal); Methodology (equal); Validation (equal); Writing – original draft (equal); Writing – review & editing (equal). **Jürgen E.K. Schawe:** Conceptualization (equal); Formal analysis (equal); Investigation (equal); Methodology (equal); Validation (equal); Writing – original draft (equal); Writing – review & editing (equal). **Peter G Weidler:** Formal analysis (equal); Investigation (equal); Methodology (equal); Validation (equal); Writing – original draft (supporting); Writing – review & editing (supporting). **Michalis Charilaou:** Validation (equal); Writing – original draft (supporting); Writing – review & editing (supporting). **Jörg F. Löffler:** Conceptualization (equal); Funding acquisition (lead); Validation (equal); Writing – original draft (supporting); Writing – review & editing (supporting). **Andreas U. Gehring:** Conceptualization (equal); Formal analysis (equal); Investigation (equal); Methodology (equal); Validation (equal); Writing – original draft (equal); Writing – review & editing (equal).

DATA AVAILABILITY

The data that support the findings of this study are openly available in the ETH Research collection at https://doi.org/10.3929/ethz-b-000565700, Supplemental material to the paper "Anisotropy-induced spin disorder in intergrown, ferrimagnetic Fe7S8 polytypes."

REFERENCES

[1]G. Rahman, V. M. García-Suárez, and S. C. Hong, "Vacancy-induced magnetism in SnO_2: A density functional study," Phys. Rev. B **78**, 184404 (2008).
[2]A. M. Valencia and M. J. Caldas, "Single vacancy defect in graphene: Insights into its magnetic properties from theoretical modeling," Phys. Rev. B **96**, 125431 (2017).
[3]Y. Zhang and H. Liu, "Study on the structure, vacancy defect, and magnetic properties for $Gd_{1-x}Ce_xMnO_3$ ceramics," J. Supercond. Nov. Magn. **34**, 3229–3236 (2021).
[4]H. Wang and I. Salveson, "A review on the mineral chemistry of the non-stoichiometric iron sulphide, $Fe_{1-x}S$ ($0 \leq x \leq 0.125$): polymorphs, phase relations and transitions, electronic and magnetic structures," Phase Transitions **78**, 547–567 (2005).
[5]E. F. Bertaut, "Contribution à l'étude des structures lacunaires: La pyrrhotine," Acta Cryst. **6**, 557–561 (1953).
[6]A. Nakano, M. Tokonami, and N. Morimoto, "Refinement of 3C pyrrhotite, Fe_7S_8," Acta Crystallogr., Sect. B **35**, 722–724 (1979).
[7]C. Aubourg, M. Jackson, M. Ducoux, and M. Mansour, "Magnetite-out and pyrrhotite-in temperatures in shales and slates," Terra Nova **31**, 534–539 (2019).
[8]D. L. Schrader and T. J. Zega, "Petrographic and compositional indicators of formation and alteration conditions from LL chondrite sulfides," Geochim. Cosmochim. Acta **264**, 165–179 (2019).
[9]T. O'Brien, J. A. Tarduno, A. Anand *et al.*, "Arrival and magnetization of carbonaceous chondrites in the asteroid belt before 4562 million years ago," Commun. Earth Environ. **1**, 54 (2020).
[10]M. Pósfai, T. G. Sharp, and A. Kontny, "Pyrrhotite varieties from the 9.1 km deep borehole of the KTB project," Am. Mineral. **85**, 1406–1415 (2000).
[11]C.-S. Horng, "Unusual magnetic properties of sedimentary pyrrhotite in methane seepage sediments: Comparison with metamorphic pyrrhotite and sedimentary greigite," J. Geophys. Res. Solid Earth **123**, 4601–4617, https://doi.org/10.1002/2017JB015262 (2018).
[12]F. W. Herbert, A. Krishnamoorthy, B. Yildiz, and K. J. Van Vliet, "Diffusion-limited kinetics of the antiferromagnetic to ferrimagnetic λ-transition in $Fe_{1-x}S$," Appl. Phys. Lett. **106**, 092402 (2015).
[13]A. V. Powell, P. Vaqueiro, K. S. Knight, L. C. Chapon, and R. D. Sánchez, "Structure and magnetism in synthetic pyrrhotite Fe_7S_8: A powder neutron-diffraction study," Phys. Rev. B **70**, 014415 (2004).
[14]F. Keller-Besrest, G. Collin, and R. Comès, "Structure and planar faults in the defective NiAs-type compound 3c Fe_7S_8," Acta Crystallogr., Sect. B **39**, 296–303 (1983).
[15]W. Wang, F. Li, F. Zhao, J. Wang, and G. Zhao, "Magnetic properties and Mössbauer spectra of Fe_7S_8 nanorods," Int. J. Nanosci. **11**, 1250036 (2012).
[16]Q. He, K. Rui, J. Yang, and Z. Wen, "Fe_7S_8 nanoparticles anchored on nitrogen-doped graphene nanosheets as anode materials for high-performance sodium-ion batteries," ACS Appl. Mater. Interfaces **10**, 29476–29485 (2018).
[17]H. Li, Y. Ma, H. Zhang *et al.*, "Metal–organic framework derived Fe_7S_8 nanoparticles embedded in heteroatom-doped carbon with lithium and sodium storage capability," Small Methods **4**, 2000637 (2020).
[18]H. Haraldsen, "Über die Eisen (II)-Sulfidmischkristalle," Z Anorg. Allg. Chem. **246**, 169–194 (1941).
[19]M. G. Townsend, A. H. Webster, J. L. Horwood, and H. Roux-Buisson, "Ferrimagnetic transition in $Fe_{0.9}S$: Magnetic, thermodynamic and kinetic aspects," J. Phys. Chem. Solids **40**, 183–189 (1979).
[20]D. Koulialias, P. G. Weidler, M. Charilaou, J. F. Löffler, and A. U. Gehring, "Cation diffusion patterns across the magneto-structural transition in Fe_7S_8," Phys. Chem. Chem. Phys. **21**, 13040–13046 (2019).
[21]D. Koulialias, J. E. K. Schawe, J. F. Löffler, and A. U. Gehring, "Structural relaxation in layered, non-stoichiometric Fe_7S_8," Phys. Chem. Chem. Phys. **23**, 1165–1171 (2021).
[22]D. Koulialias, E. Canévet, M. Charilaou *et al.*, "The relation between local structural distortion and the low-temperature magnetic anomaly in Fe_7S_8," J. Phys. **30**, 425803 (2018).
[23]A. U. Gehring, A. Firlus, D. Koulialias, P. G. Weidler, and J. F. Löffler, "The Besnus transition in 4C pyrrhotite revisited," Geophys. J. Int. **228**, 1724–1730 (2022).
[24]M. Tokonami, K. Nishiguchi, and N. Morimoto, "Crystal structure of a monoclinic pyrrhotite (Fe_7S_8)," Am. Mineral. **57**, 1066–1080 (1972).
[25]L. Néel, "Some new results on antiferromagnetism and ferromagnetism," Rev. Mod. Phys. **25**, 58–63 (1953).
[26]C. R. S. Haines, C. J. Howard, R. J. Harrison, and M. A. Carpenter, "Group-theoretical analysis of structural instability, vacancy ordering and magnetic transitions in the system troilite (FeS)–pyrrhotite ($Fe_{1-x}S$)," Acta Crystallogr., Sect. B **75**, 1208–1224 (2019).
[27]P. Weiss, "Sur l'aimantation plane de la pyrrhotine," J. Phys. Theor. Appl. **8**, 542–544 (1899).
[28]J. B. Goodenough, *Magnetism and the Chemical Bond* (Wiley, 1963).
[29]A. Živković, H. E. King, M. Wolthers, and N. H. de Leeuw, "Magnetic structure and exchange interactions in pyrrhotite end member minerals: Hexagonal FeS and monoclinic Fe_7S_8," J. Phys. **33**, 465801 (2021).
[30]M. Bin and R. Pauthenet, "Magnetic anisotropy in pyrrhotite," J. Appl. Phys. **34**, 1161–1162 (1963).
[31]M. J. Besnus and A. J. P. Meyer, "Nouvelles données exp érimentales sur le magnétisme de la pyrrhotine naturelle," in *Proceedings of the International Conference on Magnetism* (Institute of Physics, 1964), pp. 507–511.
[32]G. Fillion and P. Rochette, "The low temperature transition in monoclinic pyrrhotite," J. Phys. Colloq. **49**, C8-907–C8-908 (1988).
[33]K. Adachi, "Origine de l'énergie d'anisotropie magnétocristalline de la pyrrhotine," J. Phys. **24**, 725–731 (1963).
[34]D. Koulialias, M. Charilaou, R. Schäublin *et al.*, "Ordered defects in $Fe_{1-x}S$ generate additional magnetic anisotropy symmetries," J. Appl. Phys. **123**, 033902 (2018).
[35]D. Koulialias, M. Charilaou, C. Mensing, J. F. Löffler, and A. U. Gehring, "Torque analysis of incoherent spin rotation in the presence of ordered defects," Appl. Phys. Lett. **112**, 202404 (2018).
[36]M. Charilaou, J. Kind, D. Koulialias *et al.*, "Magneto-electronic coupling in modulated defect-structures of natural $Fe_{1-x}S$," J. Appl. Phys. **118**, 083903 (2015).
[37]L. Jin, D. Koulialias, M. Schnedler *et al.*, "Atomic-scale characterization of commensurate and incommensurate vacancy superstructures in natural pyrrhotites," Am. Mineral. **106**, 82–96 (2021).
[38]R. W. Cheary and A. Coelho, "A fundamental parameters approach to x-ray line-profile fitting," J. Appl. Crystallogr. **25**, 109–121 (1992).
[39]Bruker AXS GmbH, *TOPAS4.2 User Manual* (Bruker AXS GmbH, 2009).
[40]A. D. Elliot, "Structure of pyrrhotite 5C (Fe_9S_{10})," Acta Crystallogr., Sect. B **66**, 271–279 (2010).
[41]D. Koulialias, "Magnetic thermodynamics of natural monoclinic pyrrhotite," Ph.D disseration (ETH Zurich, 2019).
[42]M. W. R. Volk, E. McCalla, B. Voigt *et al.*, "Changes in physical properties of 4*C* pyrrhotite (Fe_7S_8) across the 32 K Besnus transition," Am. Mineral. **103**, 1674–1689 (2018).
[43]S. Havriliak and S. Negami, "A complex plane analysis of α-dispersions in some polymer systems," J. Polym. Sci. **14**, 99–117 (1966).
[44]E. R. Kassner, A. B. Eyvazov, B. Pichler *et al.*, "Supercooled spin liquid state in the frustrated pyrochlore $Dy_2Ti_2O_7$," Proc. Natl. Acad. Sci. U. S. A. **112**, 8549–8554 (2015).
[45]E. Schlosser and A. Schönhals, "Dielectric relaxation in polymer solids Part 2: Application of the new model to polyurethane systems," Colloid Polym. Sci. **267**, 133–138 (1989).
[46]A. Schönhals and E. Schlosser, "Dielectric relaxation in polymeric solids Part 1. A new model for the interpretation of the shape of the dielectric relaxation function," Colloid Polym. Sci. **267**, 125–132 (1989).
[47]R. Böhmer, K. L. Ngai, C. A. Angell, and D. J. Plazek, "Nonexponential relaxations in strong and fragile glass formers," J. Chem. Phys. **99**, 4201–4209 (1993).
[48]C. A. Angell, "Perspective on the glass transition," J. Phys. Chem. Solids **49**, 863–871 (1988).
[49]L. M. C. Janssen, "Mode-coupling theory of the glass transition: A primer," Front. Phys. **6**, 97 (2018).